JOURNAL OF MATERIALS SCIENCE 17 (1982) 1689–1699

The development of surface topography using two ion beams

S. S. MAKH, R. SMITH, J. M. WALLS
Loughborough University of Technology, Loughborough, Leicestershire, UK

Ion etching is a well-established technique for the micromachining of solid surfaces. It is used extensively in surface analysis with techniques such as Auger electron spectroscopy, ESCA and SIMS, both for surface cleaning and composition–depth profiling. In all of these applications the formation of ion-induced surface topography is a serious problem. Experimental evidence has shown that the use of two ion guns symmetrically inclined about the surface normal can partially ameliorate this difficulty. This paper considers the problem theoretically and shows for model systems the type of topography produced by two guns for various angles of separation. In general, the use of two guns suppresses cone formation and leads to the development of flatter-topped structures. Two guns also tend to undercut impurities which would otherwise lead to massive cone formation using one ion gun. The analysis lends further support to the use of twin ion beams for optimum sputter-depth profiling in surface analysis.

1. Introduction

It is well known that during ion etching of solids certain well-defined features such as cones and pits can be formed [1, 2]. The formation of such topography is deleterious to many applications of ion etching including the micromachining of surface relief on electronic devices and in sputter-depth profiling in surface analysis [3, 4]. The nucleation of ion-induced topography on surfaces can be caused by a number of mechanisms. It can be caused, for example, by the occurrence of impurities, implanted gas, initial surface roughness, and in the case of crystalline materials, by the formation of ion-induced crystal defects [5–7]. Once the topography is nucleated, it is further modified since the erosion rate at each point on the surface is a sensitive function of ion-incidence angle.

In principle, ion-induced topography could be minimized by rotating the sample surface so that it subtends all angles of incidence to the ion beam. Unfortunately in many applications, and particularly those involving ultra-high vacuum, this is not practicable. However, Sykes *et al.* [8] have recently reported that the depth resolution of composition–depth profiles using Auger electron spectroscopy can be improved when two ion guns are employed, each aligned symmetrically about the sample normal with each delivering the same ion current. It has been interpreted that the effect of using two ion guns is to suppress the formation of ion-induced surface topography [8]. In this paper a theoretical analysis is presented which supports this view and which allows the mechanisms involved to be more fully understood.

The theory of evolution of surface shape during ion bombardment has been considered by many authors [9–13]. Stewart and Thompson [9] first considered the rectilinear motion of points on a surface and showed that eroding planes could intersect to form wedges. Barber *et al.* [10] developed a graphical method of predicting how two-dimensional surfaces erode by applying the theory of crystal dissolution. Nobes *et al.* [11] and Carter *et al.* [12] have developed a theory which follows the differential motion of points on a surface in two dimensions. Recently, Smith and Walls [13] have formulated a general three-dimensional theory of surface erosion employing the method of characteristics which can be used to predict the effects of non-uniform ion current distributions and which is convenient for subsequent numerical calculations and computer

0022–2461/82/061689–11$03.82/0

simulation. The theory has also been used to predict the effects of crystallinity [14, 15] and in a modified form can account for the build-up of material by redeposition [16]. In this paper, general equations are derived to predict the development of surface shape during bombardment using two ion beams. As an example to illustrate the method, the equations are used to simulate the development in shape of an initially circular cross-section during ion bombardment with two ion beams and the results compared with a similar simulation using one ion beam.

2. Theoretical model

Consider an element of surface AB, shown schematically in two dimensions in Fig. 1, exposed to two uniform fluxes of energetic ions, ϕ_1 and ϕ_2 per unit area per sec, incident at angles of α and β to the surface normal at A. It is assumed that the erosion of this surface is controlled by the variation of sputtering yield, S, with the ion-incidence angles α and β normal to the surface. The sputtering yield is defined as the number of atoms removed from the surface per incident ion. A typical relationship between $S(\theta)$ and θ for an amorphous surface in the range $0 \leqslant \theta \leqslant \pi/2$ is shown in Fig. 2. It can be seen that $S(\theta)$ has a minimum value of $S(0)$ at $\theta = 0$, rising to a maximum and then decreasing to zero at $\theta = \pi/2$.

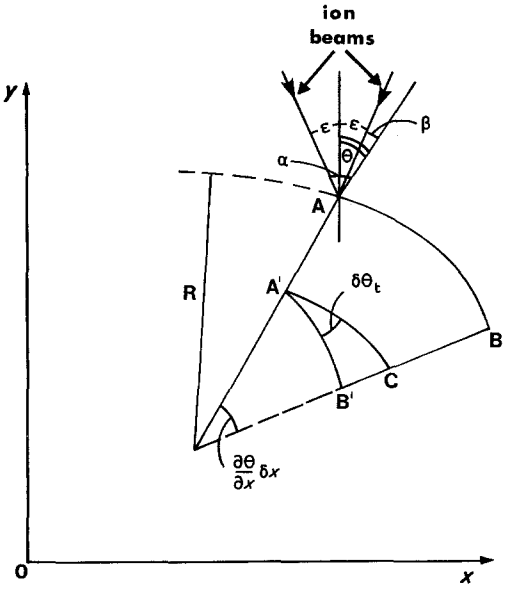

Figure 1 A schematic diagram illustrating the bombardment of the section AB, at time t, of a surface contour in two dimensions and its erosion to A'B' at time $t + \delta t$.

Let $S_1(\alpha)$ and $S_2(\beta)$ respectively be the sputtering yields for the beams incident at angles α and β to the surface normal. The y-direction is defined along the angle bisector of the beam directions so that the ion beams are placed about this line. Let the angle made by the beams to the y-direction be ϵ. Then $\alpha = \theta + \epsilon$ and $\beta = \theta - \epsilon$. In a time δt, the surface erodes by a distance δr, in a direction perpendicular to the surface. Thus

$$\frac{\partial r}{\partial t} = \frac{1}{N}[\phi_1 S_1(\alpha)\cos\alpha + \phi_2 S_2(\beta)\cos\beta], \quad (1)$$

where N is the atomic density of the target. Now consider erosion in two dimensions as shown in Fig. 1. In a time δt, A and B erode to A' and B' respectively where AA' and BB' are perpendicular to the tangents at A and B. For the element AB in Fig. 1, the tangential angles increase from α and β at A to $[\alpha + (\partial\theta/\partial x)\delta x]$ and $[\beta + (\partial\theta/\partial x)\delta x]$ at B. Thus, using Equation 1 we have to a first order approximation

$$AA' = \frac{1}{N}[\phi_1 S_1(\alpha)\cos\alpha + \phi_2 S_2(\beta)\cos\beta]\delta t, \quad (2)$$

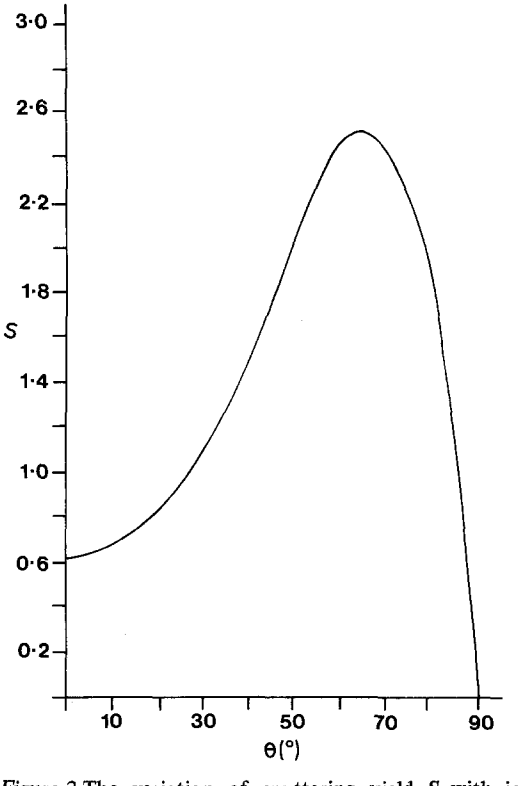

Figure 2 The variation of sputtering yield S with ion-incidence angle θ.

and

$$BB' = \frac{1}{N}\left[\phi_1 S_1\left(\alpha + \frac{\partial\theta}{\partial x}\delta x\right)\cos\left(\alpha + \frac{\partial\theta}{\partial x}\delta x\right)\right] + \phi_2 S_2\left[\left(\beta + \frac{\partial\theta}{\partial x}\delta x\right)\cos\left(\beta + \frac{\partial\theta}{\partial x}\delta x\right)\right]\delta t. \quad (3)$$

If A'C is drawn parallel to AB, then

$$CB' = \frac{1}{N}\frac{\partial\theta}{\partial x}\delta x\frac{d}{d\theta}(\phi_1 S_1\cos\alpha + \phi_2 S_2\cos\beta)\,\delta t, \quad (4)$$

where $S_1 \equiv S_1(\alpha)$ and $S_2 \equiv S_2(\beta)$.

Also $A'C = R(\partial\theta/\partial x)\delta x$, where R is the radius of curvature of AB. Now $\delta\theta_t$ is the change in tangential angle from A to A' in time δt, therefore

$$\frac{\delta\theta_t}{\delta t} = \frac{CB'}{A'C} = \frac{1}{NR}\frac{d}{d\theta}(\phi_1 S_1\cos\alpha + \phi_2 S_2\cos\beta). \quad (5)$$

where

$$S_1' = \frac{dS_1(\alpha)}{d\theta} \quad \text{and} \quad S_2' = \frac{dS_2(\beta)}{d\theta}. \quad (10)$$

Conversely, if θ is a function only of y and time, then

$$\frac{\delta\theta}{\delta t} = \left(\frac{\partial\theta}{\partial y}\right)_t\frac{\delta y}{\delta t} + \left(\frac{\partial\theta}{\partial t}\right)_y \quad (11)$$

and using 5 it can be shown that

$$\left(\frac{\partial\theta}{\partial t}\right)_y\left(\frac{\partial\theta}{\partial y}\right)_t^{-1} = -\frac{1}{N}[\sin\theta(\phi_1 S_1'\cos\alpha + \phi_2 S_2'\cos\beta) - (\phi_1 S_1 + \phi_2 S_2)\cos\epsilon]. \quad (12)$$

Equations 9 and 12 give the rate of motion of points along a characteristic line in (x, t) and (y, t) space, respectively. Division of Equation 12 by Equation 9 gives the slope of the characteristic line in (x, y) space, i.e.,

$$\left|\frac{\partial y}{\partial x}\right|_\theta = -\left[\frac{\sin\theta\{\phi_1 S_1'\cos\alpha + \phi_2 S_2'\cos\beta\} - (\phi_1 S_1 + \phi_2 S_2)\cos\epsilon}{\cos\theta\{\phi_1 S_1'\cos\alpha + \phi_2 S_2'\cos\beta\} + (\phi_2 S_2 - \phi_1 S_1)\sin\epsilon}\right] \quad (13)$$

This expresses the rate of change of tangential angle in the direction of the surface normal. Now consider θ to be a function only of x and time. Then

$$\delta\theta = \left(\frac{\partial\theta}{\partial x}\right)_t\delta x + \left(\frac{\partial\theta}{\partial t}\right)_x\delta t \quad (6)$$

and so

$$\frac{\delta\theta}{\delta t}\text{ in any direction} = \left(\frac{\partial\theta}{\partial x}\right)_t\frac{\delta x}{\delta t} + \left(\frac{\partial\theta}{\partial t}\right)_x. \quad (7)$$

The above equation expresses the rate of change of θ in any direction. If we choose this direction to be the normal direction n then, using Equation 5, we have

$$\frac{1}{NR}\frac{d}{d\theta}(\phi_1 S_1\cos\alpha + \phi_2 S_2\cos\beta) = \left(\frac{\partial\theta}{\partial x}\right)_t\left(\frac{\partial x}{\partial t}\right)_n + \left(\frac{\partial\theta}{\partial t}\right)_x. \quad (8)$$

After some manipulation it can be shown that

$$\left(\frac{\partial\theta}{\partial t}\right)_x\left(\frac{\partial\theta}{\partial x}\right)_t^{-1} = \frac{1}{N}[\cos\theta(\phi_1 S_1'\cos\alpha + \phi_2 S_2'\cos\beta) + (\phi_2 S_2 - \phi_1 S_1)\sin\epsilon], \quad (9)$$

Equations 9 and 12 are standard partial differential equations which are solved by writing down their auxiliary equations. For example, Equation 9 can be rewritten as

$$\left(\frac{\partial\theta}{\partial t}\right)_x - G\left(\frac{\partial\theta}{\partial x}\right)_t = 0, \quad (14)$$

where

$$G = \frac{1}{N}[\cos\theta\{\phi_1 S_1'\cos\alpha + \phi_2 S_2'\cos\beta\} + (\phi_2 S_2 - \phi_1 S_1)\sin\epsilon]. \quad (15)$$

Auxiliary equations are

$$\frac{dt}{1} = \frac{dx}{-G} = \frac{d\theta}{0}, \quad (16)$$

therefore along the characteristics

$$\frac{dx}{dt} = -G = -\frac{1}{N}[\cos\theta\{\phi_1 S_1'\cos\alpha + \phi_2 S_2'\cos\beta\} + (\phi_2 S_2 - \phi_1 S_1)\sin\epsilon], \quad (17)$$

and θ is constant, as for one beam erosion.

Thus the characteristic lines are lines of constant surface orientation whose gradients in the

x–y plane are given by Equation 13. The co-ordinate x on the sputtered surface is related to its value x_0 before bombardment, by

$$x = x_0 - \frac{t}{N}[\cos\theta\{\phi_1 S_1' \cos\alpha + \phi_2 S_2' \cos\beta\} + (\phi_2 S_2 - \phi_1 S_1)\sin\epsilon]. \quad (18)$$

Going through a similar procedure using Equation 12 gives the variation of y along the characteristics,

$$y = y_0 + \frac{t}{N}[\sin\theta\{\phi_1 S_1' \cos\alpha + \phi_2 S_2' \cos\beta\} - (\phi_1 S_1 + \phi_2 S_2)\cos\epsilon]. \quad (19)$$

If ϵ is put equal to zero and $\phi_1 = \phi_2 = \phi/2$, then Equations 18 and 19 reduce to the equations for a single beam of energetic ions, ϕ per unit area per sec, incident along the negative y-direction. Equation 13 gives the direction of motion of points of constant surface orientation as the surface is sputtered. The speed of motion of such points is determined using Equations 18 and 19, i.e.,

$$v^2 = \left(\frac{\partial x}{\partial t}\right)_\theta^2 + \left(\frac{\partial y}{\partial t}\right)_\theta^2, \quad (20)$$

hence, from Equations 18 and 19

$$v^2 = \frac{1}{N^2}\left\{\left[\frac{\mathrm{d}}{\mathrm{d}\theta}(\phi_1 S_1 \cos\alpha + \phi_2 S_2 \cos\beta)\right]^2 + (\phi_1 S_1 \cos\alpha + \phi_2 S_2 \cos\beta)^2\right\}. \quad (21)$$

Now the rate of erosion of the surface by sputtering along the normal direction is $1/N(\phi_1 S_1 \cos\alpha + \phi_2 S_2 \cos\beta)$ from Equation 1. Denote this normal erosion by ρ, then

$$v^2 = \left(\frac{\partial \rho}{\partial \theta}\right)^2 + \rho^2, \quad (22)$$

as shown by Carter *et al.* [17] for erosion of one beam.

To determine the condition for the formation of edges, consider two points close together on the initial surface contour, with co-ordinates (x_0, y_0) and $(x_0 + \delta x_0, y_0 + \delta y_0)$ and with orientations θ and $\theta + \delta\theta$. Suppose after a time, t, these have eroded to the points (x_t, y_t) and (x_{td}, y_{td}). From Equation 6

$$x_t = x_0 - \frac{t}{N}[\cos\theta\{\phi_1 S_1' \cos\alpha + \phi_2 S_2' \cos\beta\} + (\phi_2 S_2 - \phi_1 S_1)\sin\epsilon], \quad (23)$$

and

$$x_{td} = x_0 + \delta x_0 - \frac{t}{N}\{\cos(\theta + \delta\theta)[\phi_1 S_1'(\alpha + \delta\theta) \times \cos(\alpha + \delta\theta) + \phi_2 S_2'(\beta + \delta\theta)\cos(\beta + \delta\theta)] + [\phi_2 S_2(\beta + \delta\theta) - \phi_1 S_1(\alpha + \delta\theta)]\sin\epsilon\}. \quad (24)$$

The radius of curvature of the initial surface at (x_0, y_0) is given by

$$\delta x_0 \simeq R_0 \cos\theta\delta\theta, \quad (25)$$

and after a time, t, by

$$x_{td} - x_t \simeq R_t \cos\theta\delta\theta. \quad (26)$$

Thus subtracting Equation 23 from Equation 24 and expanding to first order in $\delta\theta$ gives

$$R_t = R_0 - \frac{t}{N}[\phi_1 S_1'' \cos\alpha + \phi_2 S_2'' \cos\beta - 2(\phi_1 S_1' \sin\alpha + \phi_2 S_2' \sin\beta)], \quad (27)$$

where

$$S_1'' = \frac{\mathrm{d}^2 S_1(\alpha)}{\mathrm{d}\theta^2} \quad \text{and} \quad S_2'' = \frac{\mathrm{d}^2 S_2(\beta)}{\mathrm{d}\theta^2}. \quad (28)$$

Thus, R_t varies linearly with time along the characteristics.

Edges due to the intersection of the characteristics can form initially when $R_t = 0$ on one surface at a time

$$t = \frac{NR_0}{\phi_1 S_1'' \cos\alpha + \phi_2 S_2'' \cos\beta - 2(\phi_1 S_1' \sin\alpha + \phi_2 S_2' \sin\beta)}. \quad (29)$$

This is the same as the relationship derived by Carter *et al.* [17] for erosion by one beam.

3. Computer simulation

In this section the development of surface topography is simulated, for an initially circular cross-section, using the analysis described in the previous section. In the computer simulations it has been assumed that the ion flux of both beams is the same, viz. $\phi_1 = \phi_2 = \phi$.

The technique is as follows. First the initial profile, $y = y(x)$, is defined. The co-ordinates of a

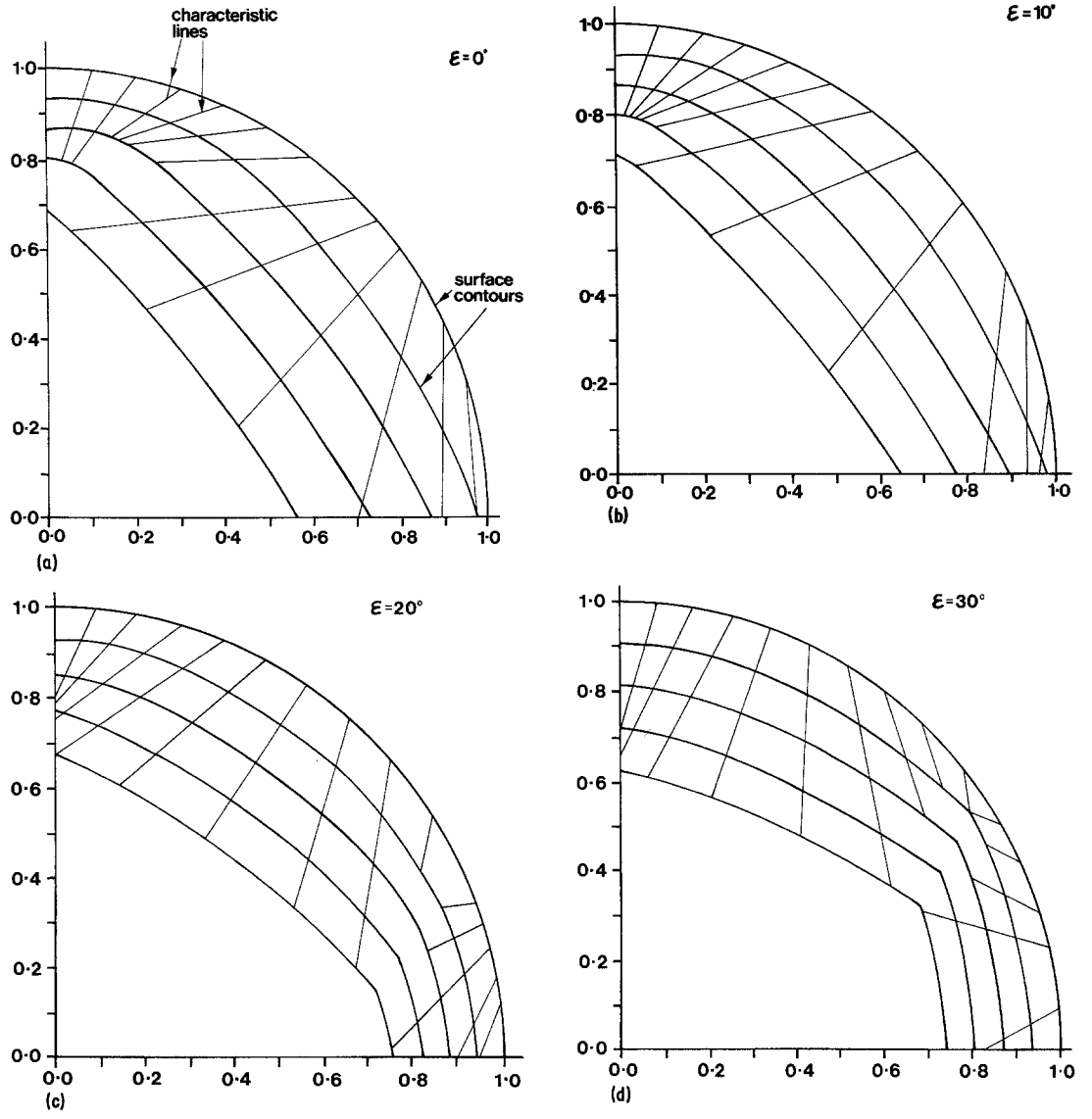

Figure 3 The erosion of a semi-circular section by two ion beams symmetrically placed about the y-axis with an angular separation, ϵ, of (a) 0°, (b) 10°, (c) 20°, (d) 30°, (e) 45°, (f) 60° and (g) 70°. The case $\epsilon = 0°$ is equivalent to erosion by one beam and illustrates the formation of a cone, but as ϵ increases flatter-topped structures are developed. There is no direct three-dimensional equivalent to these structures for $\epsilon \neq 0$ since there is no rotational symmetry.

number of points on this profile, $y_i = y(x_i)$ where $i = 1, 2, \ldots,$ are prescribed. At each of these points the angle θ, between the y-direction and the normal is calculated. Next, the angle ϵ between the beams and the y-direction is prescribed. Thus at each point the angles α and β are defined. A point on the eroded surface can then be calculated, for given values of time, using Equations 18 and 19. For uniform beams the locus of these points is a straight line, the characteristic line, which is a line of constant surface orientation. When a surface contour is bombarded by two beams, the area of bombardment is not necessarily the same as with one beam even if the beams have the same radius and the same centre. For the case of beams assumed to extend to $x = \pm\infty$, it is possible that, depending on the angle of incidence, surface protrusions can shield other parts of the surface from the beams. In the case of the erosion of a circle, some parts of the circular contour are exposed to both beams but others are eroded only by one beam. For those parts of the surface which are undergoing bombardment by both beams simultaneously the computations are evaluated using Equations 18

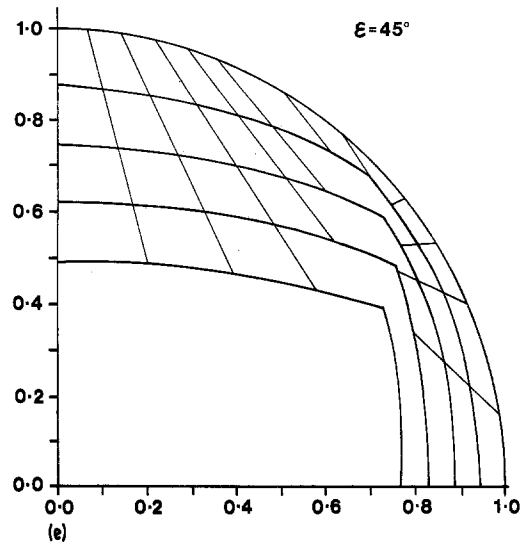

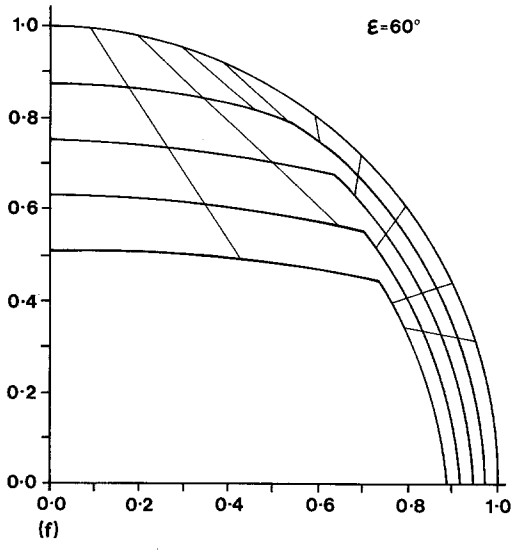

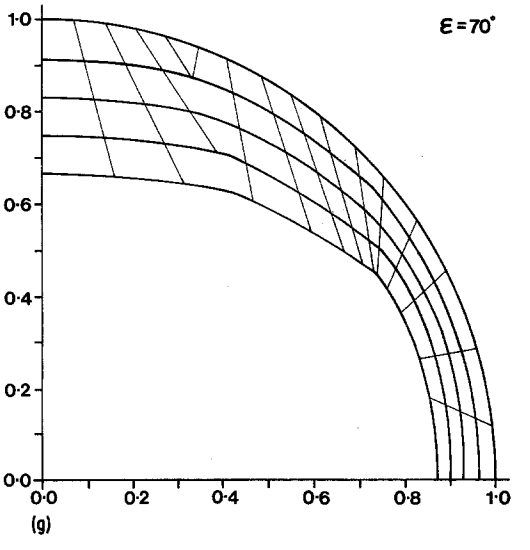

Figure 3 Continued.

and 19. The shielded parts are eroded according to bombardment by one ion beam and these equations can be derived from Equations 18 and 19 by putting ϕ_1 or ϕ_2 equal to zero. The sputtering yield, S, used in the numerical calculations is that given by Ducommum *et al.* [18] for silicon and is shown graphically in Fig. 2:

$$S(\theta) = 18.738\,45\cos\theta - 64.659\,96\cos^2\theta + 145.199\,02\cos^3\theta - 206.044\,93\cos^4\theta + 147.317\,78\cos^5\theta - 39.899\,93\cos^6\theta. \quad (30)$$

Equation 13 gives the slope of the characteristics in (x,y) space, From this it can be seen that the gradient of the characteristics will vary for each point on the initial surface. Hence some of the characteristic lines will intersect within the profile. This corresponds to the surface developing an edge. Care must be taken to ignore all points on any two characteristic lines after their point of intersection, as these points have no physical significance. In the two ion beam case, an extra edge develops at points on the surface where one of the beams becomes shielded. These edges form instantaneously unlike some edges formed by the intersection of characteristics, which form after a time given by Equation 29.

4. Results and discussion

The procedure outlined in Section 3 was carried out for a circular cross-section with the two ion beams placed symmetrically about the normal at $x = 0$. The values of ϵ chosen were 0°, 10°, 20°, 30°, 45°, 60° and 70°, to explore fully the effects of varying the angle of ion-incidence. The erosion of an initially circular cross-section as a function of ϵ, is shown in Fig. 3a to g. The results show that the type of geometry developed varies significantly with ϵ. For values of $\epsilon \leqslant 45°$ the end form is still wedge-shaped (Fig. 3a to d). However for $\epsilon \geqslant 45°$ a flat-topped formation results (Fig. 3e to g). Also, as the angle ϵ increases the lateral erosion of the hummocks decreases.

One of the most important applications of ion etching is in surface analysis and the erosion of such surfaces during depth profiling is a complex process with the constant inception of surface protrusions and pits due to impurities or intrinsic or ion-beam induced defects. Such topography is subsequently modified due to the variation of

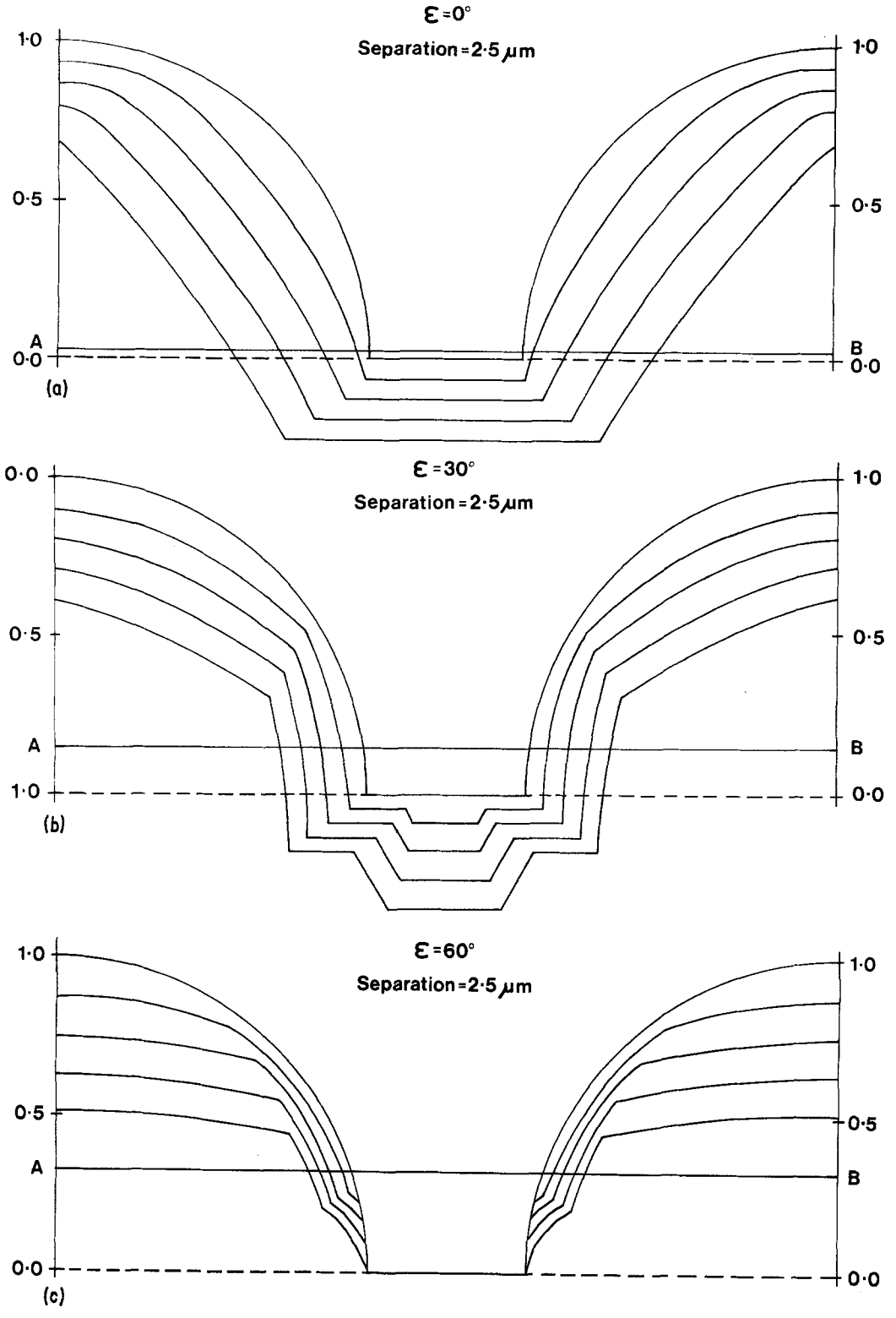

Figure 4 The erosion of two adjacent semi-circular structures of 1 μm radius and separated by 2.5 μm, by two ion beams symmetrically placed about the y-axis with an angular separation, ϵ, of (a) 0°, (b) 30° and (c) 60°. For $\epsilon = 0$ the figures illustrate the effect of shadowing on the evolution of surface shape. Note that the gradient discontinuities at the base of the structures and those induced by shadowing in (b) and (c) would in practice be smoothed out.

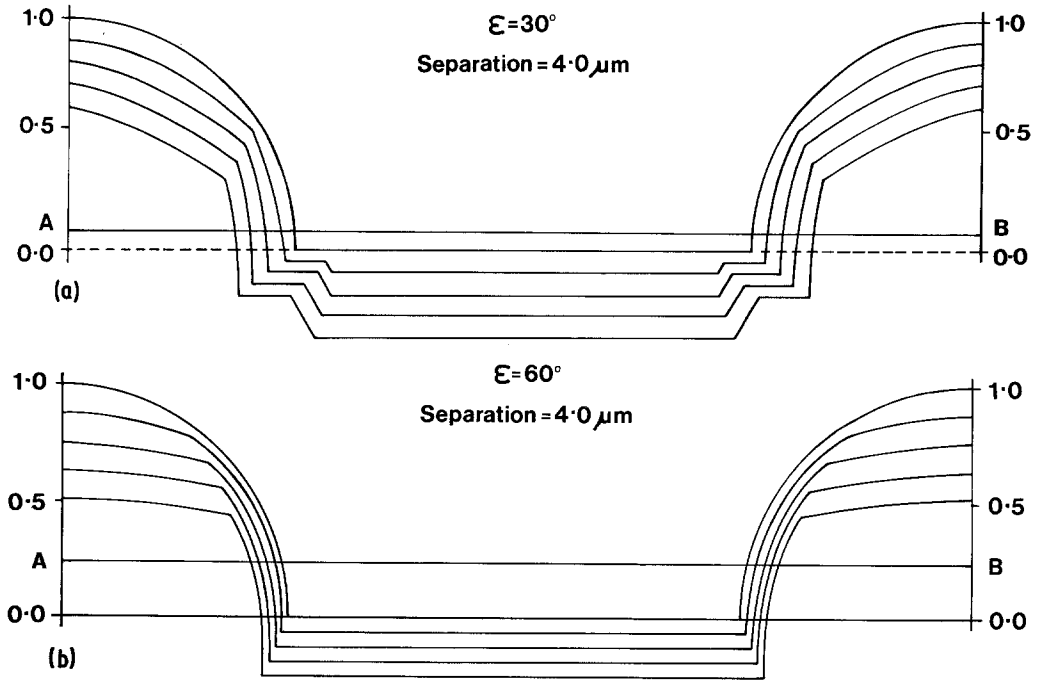

Figure 5 The erosion at two adjacent semi-circular structures of 1 μm radius and separated by 4 μm by two ion beams symmetrically placed about the y-axis with ϵ equal to (a) 30° and (b) 60°. In comparison with Fig. 4 the inversed distance between the structures reduces the influence of shadowing.

sputtering rate with ion-incidence angle. In order to determine the effects of this latter mechanism during depth profiling, a model consisting of two semi-circular protrusions above a flat plane was chosen as an initial contour and the effects of bombardment by one and two beams analysed. Fig. 4a to c shows how two such adjacent protrusions from a flat surface, subject to bombardment by two beams erode for values of ϵ or 0°, 30° and 60° respectively. The distance between the centres of the hummocks is 2.5 μm and their initial height is 1.0 μm. Fig. 4a is effectively the one ion beam case for normal incidence. In Fig. 4b the hummocks have shielded part of the intermediate flat surface from one of the ion beams. Due to this an initially flat surface has changed to a step-like structure, see Fig. 4b. In Fig. 4c the hummocks now shield each other and the intermediate surface is subject to no erosion. Fig. 5a and b shows how the hummocks erode when the distance between centres is 4.0 μm for values of ϵ of 30° and 60° respectively. In both these cases the hummocks are sufficiently far apart not to shield each other but part of the intermediate flat surface is shielded from the beams. This also leads to a surface with steps, similar to Fig. 4b.

The erosion of a surface by one ion beam, for non-normal incidence, has also been considered. Thus the topography obtained with one and two beam bombardment can be compared. Fig. 6a and b shows how the circular protrusions erode when bombarded by one ion beam at angles of 30° and 60° respectively. These illustrate that for one ion beam a wedge is always formed which points in the direction of the incident ion beam.

Finally, an attempt has been made to quantify the surface roughness obtained after bombardment of the model system by one and two beams. It has been assumed that the depth resolution can be related to the maximum deviation (d_{max}) about the average surface height. Thus the variation of d_{max} under different bombardment conditions will give a measure of how the depth resolution varies. The comparison has been made after an erosion time corresponding to depth profiling 0.26 μm of a flat plane. This shows that d_{max} is much more dependent on the angle of ion incidence than whether the surface is subjected to bombardment by one or two beams. At 60° incidence the value of d_{max} is reduced by 30% of its normal value, whereas the value of d_{max} using two beams is reduced by only about 5%, of the corresponding single beam bombardment values. Although, for the model system, the results must be treated with some

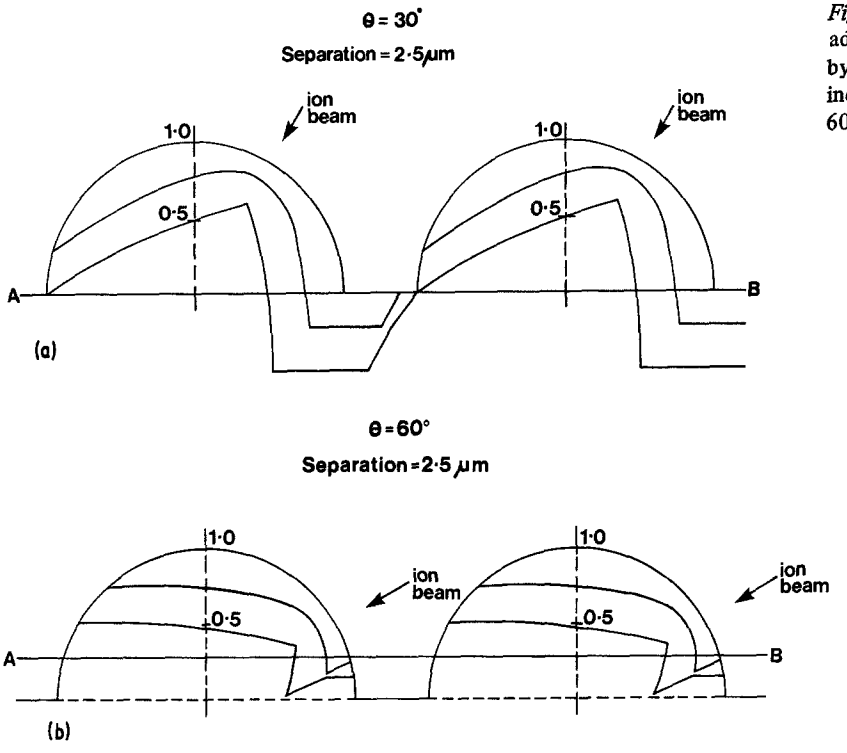

Figure 6 The erosion of two adjacent semi-circular structures by one ion beam at non-normal incidence (θ = (a) 30° and (b) 60°).

caution, they are consistent with the experimental evidence obtained by Sykes *et al.* [8] who obtained an improvement in the depth resolution using two ion guns. Fig. 7 shows a schematic diagram illustrating the geometry of their ion bombardment arrangement. Each gun was mounted symmetrically at ± 31.5° to the sample normal. Fig. 8 shows the surface topography that is obtained following ion bombardment with one and two ion guns. In both cases a steel surface was bombarded by 3 keV Ar^+ ions, current density 0.15 mA cm^{-2} until a depth of approximately 15 μm had been eroded. The surface eroded with two ion guns is free from ion-induced cones and this is reflected in the improvement usually observed in the depth resolution. This result can be partially explained by incorporating the slow lateral erosion of the hummocks for values of $\epsilon \neq 0°$ with the flattening of the tops of the hummocks and shielding effects.

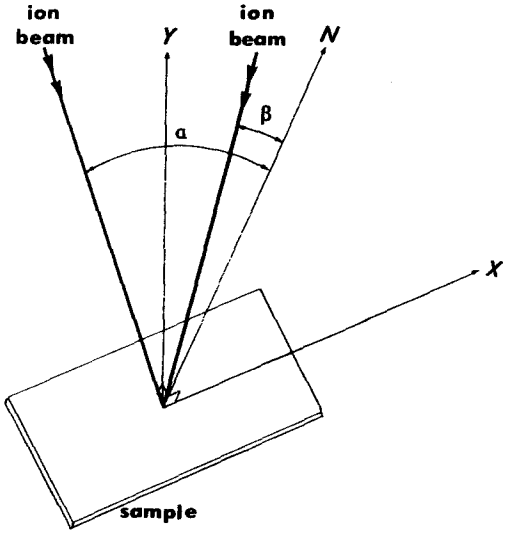

Figure 7 A schematic diagram illustrating the geometry of the twin ion beam system used in depth profiling by Auger electron spectroscopy.

In practice, massive topography on ion etched surfaces is attributed to the presence of low sputtering yield impurities or inclusions. This effect has not been considered in our model system although Figs 3a, 5 and 6 illustrate how their two-dimensional equivalents can form. Fig. 6 shows that for non-normal incidence these structures can mask substantial portions of a surface if subjected to bombardment by one ion beam alone. However, with two ion beams, this shielding is less effective and under-cutting of such conical structures will occur which will not only suppress their development but will also lead to their faster decay. This is the major reason why massive ion-induced topographical structures are not observed using two ion beams.

The type of detailed structure obtained is shown in Fig. 9. Fig. 9a shows a typical formation

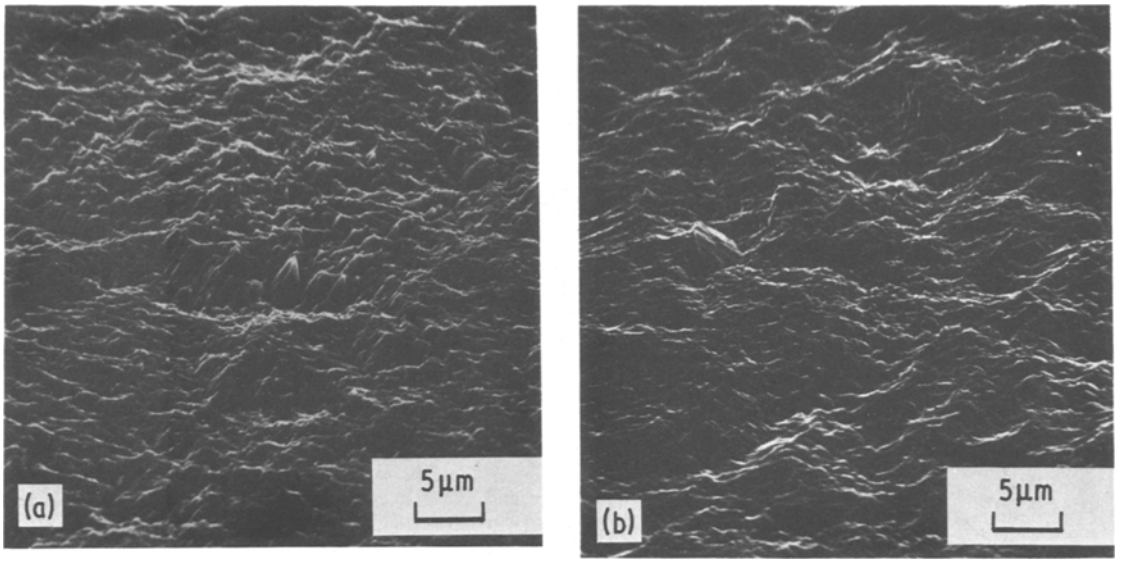

Figure 8 A comparison of the surface topography for a treated stainless steel surface, bombarded to a depth of 16 μm formed as a result of using (a) one ion gun and (b) two ion guns arranged symmetrically at 31.5° to the surface normal. Cones orientated towards the ion beam axis are clearly evident in the one gun case and completely absent in the two gun case.

of cones whose axis is along the direction of the incident ion beam. The size of these cones suggest that their origin lies in some particulate impurity or inclusion in the steel. This should be compared with Fig. 9b which shows the detailed structures obtained using two ion guns. In this case cones are not observed but a series of flat-topped structures occur similar to those predicted in the simulations shown in Fig. 3.

5. Conclusion

This paper has given a theoretical treatment for the erosion of surfaces during bombardment with two ion beams, and has accounted for the different types of topography observed. This modified topography can be used to explain the improved depth resolution of composition–depth profiles observed to occur with two ion beams on impurity-free surfaces. The improvements in depth resolu-

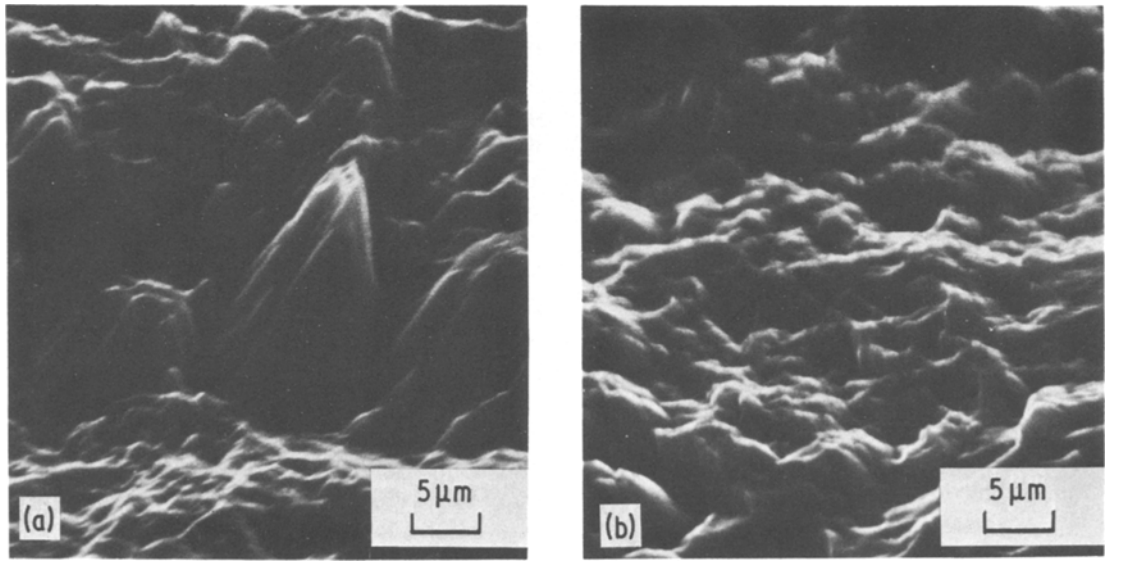

Figure 9 A comparison of the detailed structures obtained following ion erosion of a steel surface by (a) one ion gun and (b) two ion guns.

tion on surfaces which generate massive cone topography due to the presence of impurities will be due to a combination of the modified surface topography obtained using two ion beams and the under-cutting of impurities preventing the extent of cone development which occurs using one ion beam.

Acknowledgements

The authors are grateful to D. D. Hall and D. E. Sykes for useful discussions. One of the authors (SSM) is also grateful to the SRC and the Plessey Company Limited for a studentship during the tenure of which this work was undertaken.

References

1. G. K. WEHNER and D. J. HAJICEK, *J. Appl. Phys.* **42** (1971) 1145.
2. I. H. WILSON and M. W. KIDD, *J. Mater. Sci.* **6** (1971) 1362.
3. R. SMITH and J. M. WALLS, *Surface Sci.* **80** (1979) 557.
4. S. S. MAKH, R. SMITH and J. M. WALLS, *Surface Interface Anal.* **2** (1980) 115.
5. N. HERMANNE and A. ART, *Fizika* **2** (Suppl. 1) (1970) 72.
6. R. D. WEBBER and J. M. WALLS, *Thin Solid Films* **57** (1979) 201.
7. J. L. WHITTON, L. TANOVIC and J. S. WILLIAMS, *Appl. Surf. Sci.* **1** (1978) 408.
8. D. E. SYKES, D. D. HALL, R. E. THURSTANS and J. M. WALLS, *ibid.* **5** (1980) 103.
9. A. D. G. STEWART and M. W. THOMPSON, *J. Mater. Sci.* **4** (1969) 56.
10. D. J. BARBER, F. C. FRANK, M. MOSS, J. W. STEEDS and I. S. T. TSONG, *ibid.* **8** (1973) 1030.
11. M. J. NOBES, J. S. COLLIGON and G. CARTER, *ibid.* **4** (1969) 730.
12. G. CARTER, J. S. COLLIGON and M. J. NOBES, *ibid.* **6** (1971) 115.
13. R. SMITH and J. M. WALLS, *Phil. Mag.* **42** (1980) 235.
14. R. SMITH, S. S. MAKH and J. M. WALLS, Proceedings of the 4th International Conference on Solid Surfaces and Ecoss. III, Cannes, September 1980, Vol. 2 edited by D. A. Degras and M. Costa (Supplement et Le Vide, Les Couches Minces, 1980) 1209.
15. R. SMITH, T. P. VALKERING and J. M. WALLS, *Phil. Mag. A* **44** (1981) 879.
16. S. S. MAKH, R. SMITH and J. M. WALLS, in "Low Energy Ion Beams" Vol. 2, edited by I. H. Wilson and K. G. Stephens (Institute of Physics, London, 1980) p. 246.
17. G. CARTER, J. S. COLLIGON and M. J. NOBES, *Rad. Eff.* **31** (1977) 65.
18. J. P. DUCOMMUN, M. CANTAGREL and M. MOULIN, *J. Mater. Sci.* **10** (1975) 52.

Received 14 October
and accepted 4 November 1981